Received: 15 July 2023 | Revised: 19 September 2023 | Accepted: 5 October 2023

DOI: 10.1002/ppap.202300134

RESEARCH ARTICLE

PLASMA PROCESSES AND POLYMERS

Energetics of reactions in an atmospheric pressure plasma jet with argon carrier gas and hexamethyldisiloxane reagent

Giulia Laghi[1] | **Sean Watson**[2] | **Stephan Reuter**[2] | **Matteo Gherardi**[1,3] | **Michael R. Wertheimer**[2]

[1]Department of Industrial Engineering, Alma Mater Studiorum—University of Bologna, Bologna, Italy

[2]Department of Engineering Physics, Polytechnique Montreal, Montreal, Quebec, Canada

[3]Interdepartmental Centre for Industrial Research Advanced Mechanical Engineering Applications and Materials Technology, Alma Mater Studiorum—University of Bologna, Bologna, Italy

Correspondence
Michael R. Wertheimer, Department of Engineering Physics, Polytechnique Montreal, Montreal, QC H3T 1J4, Canada.
Email: michel.wertheimer@polymtl.ca

Funding information
Fonds de recherche du Québec; TransMedTech Institute; European COST Action CA20114 "Therapeutical applications of cold plasmas"; Natural Sciences and Engineering Research Council of Canada

Abstract

We report on a methodology for measuring the energy dissipated per AC high voltage cycle in a cold atmospheric pressure plasma jet (CAPJet). This method is adapted from research by Nisol et al. on plasma polymerization of hexamethyldisiloxane (HMDSO) organosilicon vapor in a large area planar dielectric barrier discharge (DBD) reactor. Here too, we measured ΔE_g, the energy difference with and without small HMDSO vapor concentrations in the argon carrier gas flow. From ΔE_g we then derived E_m, the energy per molecule, and compared values with those of Nisol. Good agreements were found, including in film structures determined from attenuated total reflectance (ATR) Fourier transform infrared (FTIR) spectra, thus suggesting that realistic E_m values can be successfully obtained also for the CAPJet case.

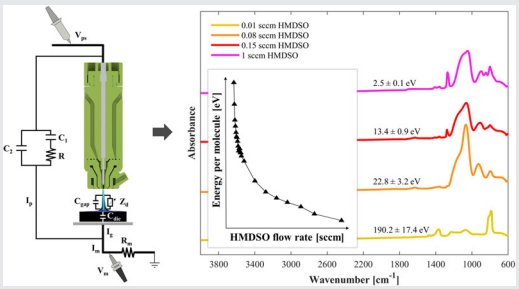

KEYWORDS

argon carrier, atmospheric pressure plasma polymerization, energy measurement, HMDSO, plasma jet

1 | INTRODUCTION

1.1 | Atmospheric pressure glow discharge (APGD) in argon (Ar)

Since the first report of APGD in helium by Bartnikas in 1968,[1] there has been an enormous expansion in the literature related to APGD, particularly in that dealing with dielectric barrier discharges (DBDs).[2] The seminal review article by Kogelschatz in 2003[2] has now been updated by another, to appear later in 2023.[3] In gases other than He, for example, the much less costly Ar, AP discharges tend to be "filamentary" (composed of many ns-duration narrow streamers) instead of "homogeneous" APGD[2] that covers

the entire electrode area. However, in 1993 Okazaki reported that a mixture of Ar with a very small amount of acetone (C_3H_6O, 3 ppm addition, for about 20 cm^2 electrode area) can lead to a stable homogeneous glow discharge.[4] Indeed, we now know that filaments can be suppressed by reducing the breakdown voltage using such so-called Penning mixtures, ones containing small concentrations of a molecular gas with an ionization energy lower than that of metastable Ar* species.[5] Besides acetone, a second gas early identified as suitable for the Penning mixture was ammonia (NH_3), for which some hundreds of ppm suffice to bring the discharge to a homogeneous regime. Fateev et al. stated that "at ammonia concentrations between 0.1% and 3%, the main processes for NH and NH_2 radical generation are energy exchange between Ar metastable atoms and ammonia molecules and Penning ionization with subsequent dissociative recombination. Collisions of electrons with ammonia molecules become important at ammonia concentrations between 3% and 10%."[6]

Since then, many other molecules have proven suitable for Penning transfer reactions from excited neutral Ar* atoms, including hexamethyldisiloxane (HMDSO),[7–9] and numerous other molecules investigated by Nisol and coworkers.[9–11] Loffhagen stated that "The Penning ionization process can play a dominant role in the production of electrons in an atmospheric-pressure low-temperature plasma and can affect the ignition voltage of such discharges." For the reaction of HMDSO with Ar* atoms, the results obtained by their model calculations agree rema rkably well with measured data of the ignition voltage and of the temporal evolution of the discharge current.[7,8] Sections in their two articles that deal with energy loss due to HMDSO collisions as a function of HMDSO concentration x (figs. 10A and 13 in Loffhagen et al.[7] and[8]), respectively, show that electron- and ion collisions play negligibly small roles compared with those with Ar* and Ar_2* for all x ($20 < x < 1570$ ppm). In other words, Penning chemistry dominates the measured energy loss mechanisms. We shall return to this in far more detail later in Section 4 of this article.

The fraction of the electrical energy fed into the AP Ar discharge that goes toward producing Ar* and Ar_2* turns out to be remarkably high, and this has led to the development of efficient DBD vacuum ultraviolet (VUV) light sources by Kogelschatz[2] and by Eden,[12] for example. Indeed, lamp efficiencies can be very high, in the range up to 40% or even more. This, combined with the effectiveness of Penning (as opposed to electronic or ionic) energy transfer to highly diluted reagent gas molecules in the Ar carrier gas stream, forms an important basis of this article's scientific content; this, too, will be the object of more detailed discussion in Section 4 further below.

1.2 | Plasma polymerization (PP)

Industrial applications of plasma processes now cover an impressively diverse spectrum of technologies, including PP.[13] An important common requirement is their economic viability, and a key aspect underlying this is energy efficiency. A parameter proposed many years ago for tuning low-pressure (LP) PP is the Yasuda parameter, defined as the discharge power W per flow rate F times M, the precursor molecular weight ($Y = W/FM$).[14,15] Low Y-values result in less fragmentation of the precursor molecules and increase the probability of retaining their functionality, while higher values have the opposite effects. In attempts to adopt Y for use in PP at atmospheric pressure (AP),[16] those authors showed that constant Y did not necessarily provide deposits of the same chemistry and morphology, unlike in LP plasma. More recently, Hegemann and coworkers[17] proposed *energy conversion efficiency*, *ECE*, as a new parameter that permits direct comparison of LP and AP experiments. This was done for the case of the much-studied organosilicon precursor ("monomer"), HMDSO[18]: "Critical" values of energy E_m (to be defined below) or "activation energy," E_a,[18] that demarcate *ECE* regimes separating different fragmentation/reaction mechanisms were found to agree remarkably well and to correlate with specific mechanisms.

Before approximately the year 2000, PP was almost exclusively carried out under LP conditions, but AP plasma processing has since then been steadily gaining acceptance in both the "pure" and "applied" science communities. An important reason is that it obviates the need for costly vacuum equipment and therefore promises greater economic rewards.[13,19–21] The PP process comprises several distinct steps: (i) activation of the organic precursor compound or "monomer" in the gas phase; (ii) transport of resulting reactive film-forming species to the substrate surface; and (iii) plasma polymer film growth at that surface. Reactors for PP at AP are generally of the planar DBD type,[9,10,19–21] but increasingly the so-called Cold AP plasma jets (hereafter CAPJet) are used on account of greater versatility when treating other than flat substrate surfaces. The latter, PP using CAPJet reactors,[22–27] is of course the subject of this present investigation, particularly as it pertains to the organosilicon precursor HMDSO; resulting film coatings are hereafter designated "PP-HMDSO." In this latter regard, some of the present authors have developed a method for measuring E_m, the energy absorbed per

monomer molecule (in eV/molec units) in a large area planar DBD pilot-scale reactor.[9–11]

A particular objective of the research reported here has been to transfer that methodology to the case of a CAPJet, also using HMDSO as an example monomer. Before describing that novel approach, it is useful to introduce one more relevant energy measuring technique that has been known and used in DBDs for several decades, the so-called Lissajous curves method[2,4,16,28,29]: Hereby, the energy consumed per cycle of the AC voltage discharge is equal to the closed loop area of voltage, V, between the two electrodes of the DBD capacitor plotted versus the charge crossing the capacitor, Q. In the present work, we have used the Lissajous curve method as a means for comparison to the proposed energy per molecule measurement method, which we will hereafter refer to as the "Delta-E method."

2 | EXPERIMENTAL METHODOLOGY

2.1 | Plasma reactor and equivalent circuit model

A schematic view of the experimental setup is shown in Figure 1. The CAPJet plasma source was a single-electrode Jet (*AlmaJet*), described in detail elsewhere.[30,31] The source was powered by the same electrical system as described by Nisol et al.[10]: The high-voltage (HV) electrode was connected to a HV power supply, comprising a variable-frequency sinusoidal AC generator (1 Hz to > 50 kHz, Hewlett-Packard 3310 A), a power amplifier (QSC Ltd., Model RMX2450), and a HV transformer (Enercon, Model LM2727-03). The AC power supply voltage, $V_{ps}(t)$, was monitored by means of an HV probe (Tektronix P6015A). The lower plate electrode was connected to the ground via a 50 Ω precision resistor, which served to measure the discharge current pulse amplitude and shape. The discharge behavior was examined at applied HV AC frequencies, f, ranging between ca. 1 and 50 kHz, voltage and current signals all being synchronously displayed using a digital storage oscilloscope (Instek GDS-2204A, 200 MHz). In turn, these data were transmitted and acquired in real-time by USB link on a PC, where they were postprocessed by MATLAB® code to calculate the true voltage across the gas gap, V_{gap},, the discharge current, I_d, and the energy per cycle, E_g.[32,33] For calculating C_{die} and C_{gap}, characteristic capacitance values in the equivalent circuit model further below, the vertical cylindrical plasma plume in the gas gap ($r = 1.5$ mm and $d = 13$ mm) and its subsequent radial spreading on the dielectric substrate surface need to be considered, see Figure 2. We return to these in more detail below.

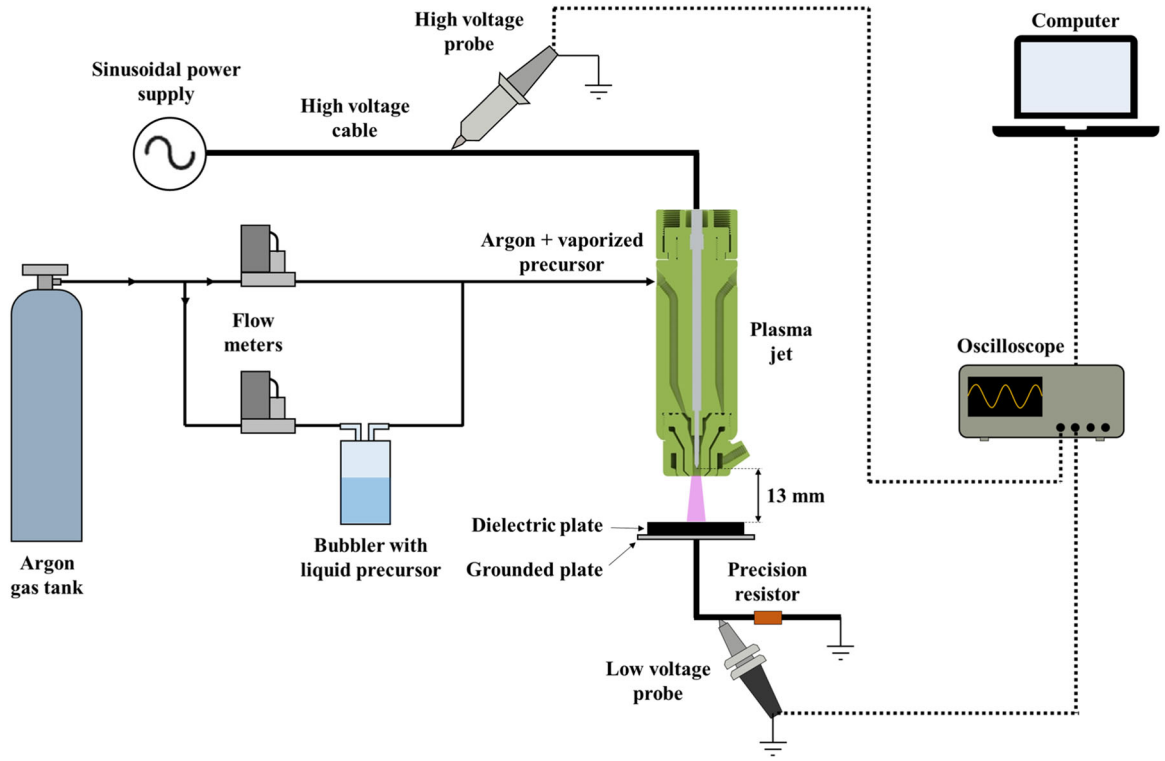

FIGURE 1 Schematic representation of the experimental setup.

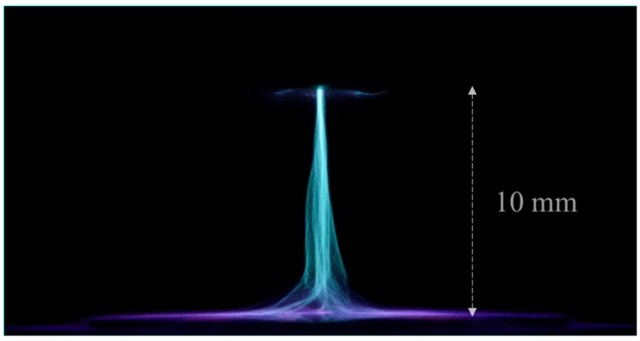

FIGURE 2 Photograph of a nearly cylindrical discharge produced with the single electrode cold atmospheric pressure plasma jet (CAPJet). The plasma plume extends another 3 mm into the plasma source (part that cannot be seen in the photograph).

The equivalent circuit model and method to calculate the energy dissipated in the gas discharge during each applied HV cycle, E_g, is described in greater detail by Nisol et al.[10] In the following, the method and circuit model will be described again briefly. A brief reminder will also be given about how two other important energy values are defined: (a) the absorbed energy difference, ΔE_g, and (b) the energy per molecule, E_m, that play key roles in the context of this research.

Figure 3b shows the equivalent electrical circuit model proposed by Nisol et al.[10] for, both, a large and smaller area DBD plasma reactor driven by a sinusoidal power source. In the present work, the same model is applied to the used CAPJet device (Figure 3a). The power supply voltage, V_{ps}, and the voltage difference across the

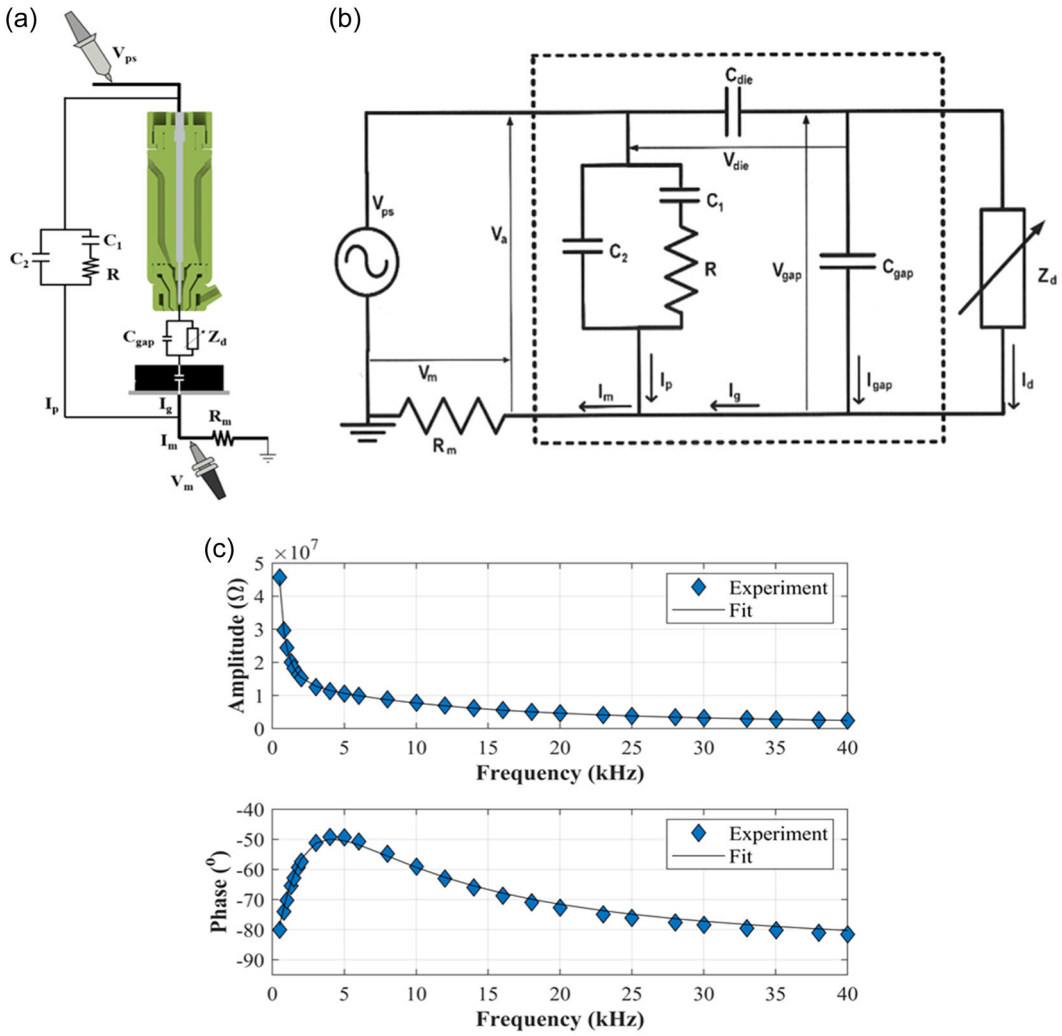

FIGURE 3 (a) Electrical equivalent circuit model applied to the single electrode plasma jet; (b) electrical equivalent circuit model for a large area dielectric barrier discharge (DBD) plasma source; (c) Z_{eq} amplitude and phase as a function of the applied high voltage (HV) frequency, f, in the absence of plasma discharge. Blue data points: experimental measurements, black continuous curve: best fit.

precision resistor, V_m, respectively, correspond to the voltage signals measured by the HV and low-voltage probes. R_m is the precision 50 Ω resistor, and Z_d is a nonlinear variable impedance that corresponds to the plasma element; its value, although unknown in precision, tends toward zero during discharges and toward infinity between them. C_{die} and C_{gap} represent characteristic capacitances of the plasma source: C_{gap} is the capacitance associated with the gas gap between the tip and the dielectric plate, while C_{die} is associated with the poly(vinyl chloride) dielectric plate. During discharges, the effective capacitance is C_{die}, while between discharges (when Z_d tends to infinity), the circuit is characterized by their series combination. Various parasitic effects present in the experimental setup are modeled by the network comprising C_2 in parallel with the series combination of C_1 and a resistor R. For calculating C_{die} and C_{gap}, we have assumed a simple columnar plasma plume in the gap, which subsequently spreads radially on the dielectric surface (Figure 2); this yields numerical values for C_{gap} and C_{die} of 0.005 pF and 1.39 pF, respectively.

To derive the remaining components C_1, C_2, and R, measurements of V_{ps} and V_m were performed in the absence of a plasma discharge, in atmospheric air at applied voltage V_{ps} =5.5 $kV_{p\text{-}p}$, for frequencies, f, varying from 0.5 up to 40 kHz. From these V_{ps} and V_m measurements, $I_m = V_m/R_m$ and the impedance of the equivalent circuit $Z_{eq} = V_{ps}/I_m$ were calculated. Amplitude and phase of Z_{eq} as a function of the frequency f are shown plotted in Figure 3c (blue data points); the best fit of these experimental data (solid black line) yields numerical values $C_1 = 5.69$ pF, $C_2 = 1.58$ pF, and $R = 14.55$ MΩ. As a first approximation, these are assumed to remain unchanged in the presence of plasma, regardless of the exact operating condition. By applying Kirchhoff's laws to the equivalent circuit in Figure 3b, we can derive the electrical energy dissipated in the gas discharge per cycle, E_g:

$$E_g = \frac{1}{n}\int V_{gap} I_d \, dt. \quad (1)$$

Here, n is the number of complete cycles at the applied voltage frequency; more details can be found in references.[32,33] The above calculations were performed in MATLAB® in the frequency domain using Fast-Fourier Transform (FFT) and inverse FFT according to.[9,10]

2.2 | Lissajous figure method

Application of the Lissajous figure method[28] was performed by replacing the 50 Ω precision resistor with a monitor capacitor, C_m, of 470 pF and by measuring the voltage across this capacitor, $V(t)$. C_m has to be chosen carefully, the assumption being that C_m placed in series does not significantly influence the overall circuit. For this assumption to be true, its value should be greater than 100 times and lower than 100,000 times that of the capacitance of the plasma source.[29] This modification in the experimental setup allowed calculating the charge accumulated on the dielectric surface, $Q(t) = C_m \times V(t)$. The energy dissipated per cycle was derived as the area of the closed loop created by plotting $Q(t)$ as a function of applied voltage, V. Note that since this method was first developed and used by Manley in the 1940s,[28] there has been criticism about its reliability; numerous very considerable improvements have therefore been proposed, for example, by Brandenburg and coworkers.[34–36] In Pipa and Brandenburg[35] they state, "The equivalent circuit approach is reliable for characterization of DBD geometries where the capacitances of the reactor do not depend on the operation conditions." Their most recent article[36] further states, "determination of the discharge voltage from charge-voltage plots and the validity of the so-called Manley power equation are revised by taking into account nonuniform coverage as well as parasitic capacitances," which they apply to evaluating energy yield of CO from splitting CO_2 in suitably designed plane-parallel DBD reactors.

2.3 | PP and characterization techniques

All experiments were performed with Ar as carrier gas (Ar, 99.999% purity, Air Liquide Canada, Ltd.), and applied HV frequency f = 20.5 kHz. The Ar flow was set to 1.5 standard liters per minute (slm), controlled by a rotameter-type flowmeter (Matheson, model 7642H, tube 605). For selected experiments, a small amount of HMDSO "monomer" vapor (in the range between F_d = 0.01 and 2 sccm) was added to the Ar carrier gas flow. For vaporizing the HMDSO, a glass bubbler (diameter = 30 mm, height = 70 mm) containing several cm^3 of the liquid precursor was fed with a suitable Ar flow, controlled by two electronic mass flow meters (MKS, model 1259B, 0–100 sccm, and 0–10 sccm N_2) and a dedicated power supply (MKS, model 247B). To precisely quantify F_d, the flow rate of the liquid reagent's (HMDSO) vapor, a calibration of mass change with time was first carried out.[9]

In this present research, PP experiments for depositing PP-HMDSO films were among the primary objectives, using both (i) a stationary substrate and (ii) one whereby back-and-forth motion at 5 mm/minute

permitted more uniform, larger area deposit, a few millimeters in width. The latter was accomplished with the motorized platen system described previously.[9,10]

To evaluate the deposition rate, a piece of single-crystal silicon (c-Si) wafer was placed on the dielectric plate, 10 mm below the CAPJet nozzle in static mode for 15 min. The thickness profile of deposited PP-HMDSO was measured with a profilometer (Bruker, DektakXT); in the top view, the resulting coating was nearly circular, and its height distribution was pseudo-Gaussian, as shown later. The thickness, d, associated with each deposition condition was the mean value at the center of the deposit, where d reached a plateau. The deposition rate was simply calculated by d divided by the deposition time of 15 min.

To determine the coatings' chemical structure and composition by attenuated total reflectance (ATR) Fourier-transform infrared (FTIR),[9] the c-Si was replaced by KBr, transparent to IR radiation. PP-HMDSO film samples were deposited on KBr (99 + %, Fisher Scientific IR grade) disc substrates of ca. 0.5 mm thickness and 13 mm diameter. ATR-FTIR spectroscopy was carried out using a Perkin Elmer infrared spectrometer with an ATR sampling accessory. Spectra were acquired in absorbance mode, from 4000 to 600 cm^{-1} with a resolution of 4 cm^{-1}. A total of 32 scans were recorded for each spectrum.

3 | EXPERIMENTAL RESULTS

3.1 | Energy measurements

Figure 4a shows a plot of the energy, E_g, absorbed by the CAPJet pure Ar plasma (black data points), determined using the method described in Section 2.1, where E_g is seen to rise quasi-linearly with increasing applied voltage, V_a, between ca. 5.5 and 9.5 kV_{p-p}. The apparently anomalous behavior between 6.5 and 8.5 kV_{p-p} is real and will be discussed further below. In the present V_a range, E_g values rise from ca. 5 to 18 μJ per period. Figure 4b shows E_g values determined by the Lissajous figures method described in Section 2.2. The values show rather similar qualitative behavior to the ones in Figure 4a, except that E_g values range from 23 to nearly 90 μJ per period.

In both Figure 4a,b, further sets of data (lower curves, red data points) correspond to the addition of 0.15 sccm HMDSO into the 1.5 slm flow of Ar carrier gas. For sufficiently low or high values of V_a [~5.5 or 9.0 kV_{p-p} in (a)], one notices near-constant gaps, ΔE_g, between the upper (*pure*) and lower (*mixed gas*) branches. Figure 5 presents plots of (a) E_g and (b) ΔE_g, both versus F_d, the HMDSO flow rate, for both $V_a = 5.5$ and 9.0 kV_{p-p}.

Returning to the observed transition over a small range of applied voltage observed in both Figure 4a,b: Below about 6.5 kV_{p-p} the ΔE_g value is significantly smaller than above about 8 kV_{p-p}, but negligible between those two V_a values. Qualitatively identical behavior has been reported for Ar with 2‰ of a hydrocarbon "monomer," C_2H_2[10] in the large area planar DBD reactor mentioned earlier. This said, the transition from a distinct low-V to a different high-V behavior appears to have a basic plasma physical explanation: We propose that this is a manifestation of the α-γ transition in high-frequency AP Ar discharges, which has been explored both experimentally and by modeling, and reported for a planar DBD reactor[37] and for a μAPPJ CAPJet.[38] Let us recall that in the so-called α-mode, bulk electrons are responsible for most electron collision processes, while in

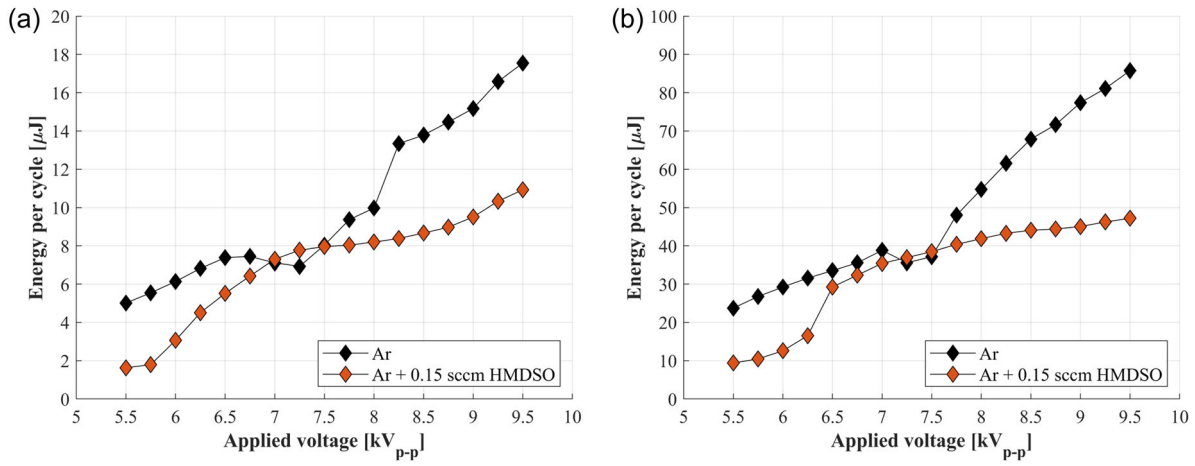

FIGURE 4 (a) Comparison of energy dissipated per cycle, E_g obtained with the present methodology, and (b) the Lissajous figures method, both in pure Ar and in the presence of HMDSO ($F_d = 0.15$ sccm) as a function of the applied voltage V_{appl} ($f = 20.5$ kHz).

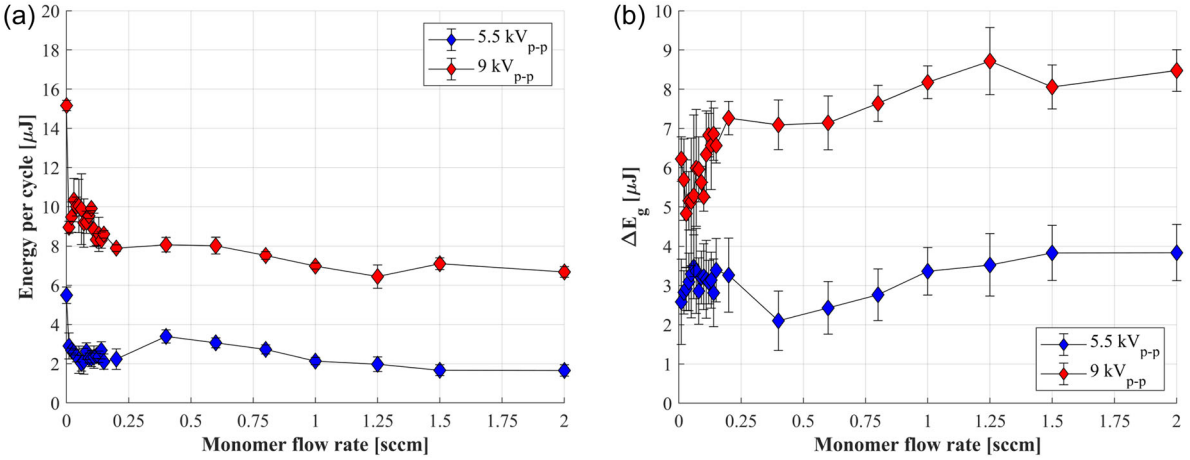

FIGURE 5 (a) Energy per voltage cycle, E_g; (b) ΔE_g, both versus hexamethyldisiloxane (HMDSO) flow rate, F_d.

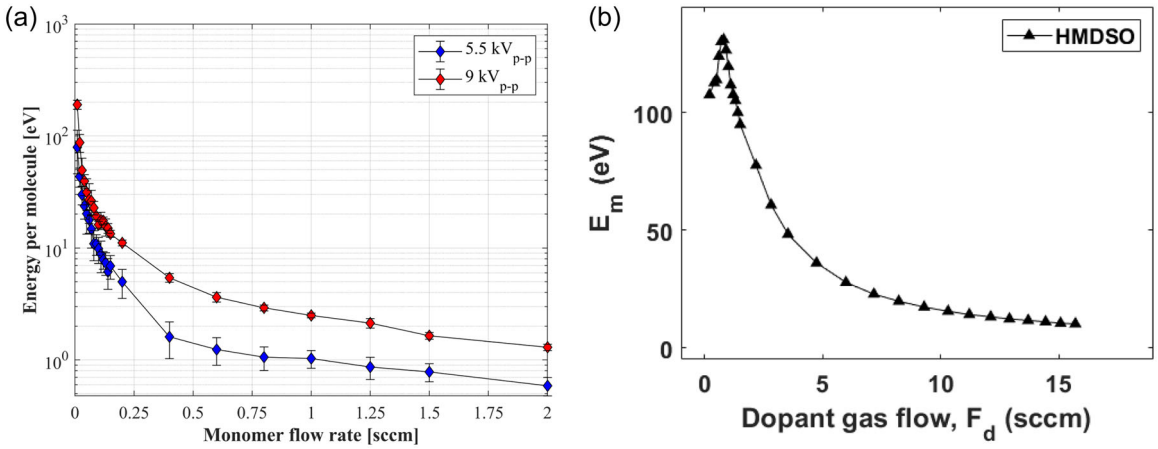

FIGURE 6 (a) logE_m versus precursor flow rate, F_d; (b) E_m versus flow rate F_d from Nisol,[9] for comparison.

the γ-mode secondary electrons largely contribute to the ionization budget.[39] Referring to Section 1.1, in[37] the Penning mixture was made up of Ar + 133 ppm of NH_3 (instead of C_2H_2[10]), and increasing the NH_3 concentration led to a decreased voltage amplitude required to reach the α-γ-mode. This latter observation was explained by an increase in the ionization rate through the Penning reaction, which enhanced ionization in the sheath. In Nisol et al.[10], doubling the discharge frequency from 20 to 40 kHz lowered the observed transition voltage from ca. 2100 to 1600 $V_{p\text{-}p}$, while in Dünnbier et al.[38], the α-γ transition voltage also decreased with rising excitation frequency. Since both these observations, variation with frequency and with "dopant" content, agree with our own experience, this would lend support to the "α-γ" interpretation we are proposing here, we believe.

Finally, from the data presented in Figure 5b, it is simple to calculate the energy per molecule, E_m, as first demonstrated by Nisol et al.[9,10]:

$$E_m\,[\text{eV/molecule}] = \frac{\Delta E_g\,[\mu\text{J}] \times 10^{-6}[\text{J}/\mu\text{J}] \times f \times 10^3[1/\text{s}] \times 6.24\text{e}^{18}[\text{eV/J}]}{N\,[\text{molecules/s}]}, \quad (2)$$

where f is the discharge frequency and N is the number of precursor molecules introduced into the discharge per second; N is calculated as shown in the following equation:

$$N\,[\text{molecules/s}] = F_d\,[\text{sccm}] \times 10^{-3}[\text{L/cm}^3] \times \frac{1}{24}[\text{mol/L}] \times N_A\,[\text{molecules/mol}] \times \frac{1}{60}[\text{min/s}], \quad (3)$$

where F_d is the precursor flow rate and N_A is the Avogadro's number.

The resulting plot is shown in Figure 6a for both $V_a = 5.5$ and 9.0 $kV_{p\text{-}p}$, where E_m is presented on a logarithmic scale on account of the large range of values from ~ 200 eV to a few eV at $F_d = 2$ sccm. For comparison, Figure 6b shows the (linear scale) E_m versus F_d plot for HMDSO taken from Nisol,[9] which displays a sharp peak at low F_d, followed by the same monotonic drop as in (a) with rising F_d values. Remarkably, the two maximum E_m values in (a) and (b), $(E_m)_{max}$, are fairly close, 190 and 131 eV, respectively; from this, one might surmise that still lower F_d in (a) might reveal a similar drop as in (b), the same (peaked) E_m versus F_d characteristic observed for all monomers.[9,10] We shall return to this in the Section 4.

3.2 | PP-HMDSO characterization results

3.2.1 | Deposition kinetics

Figure 7a, a top view of a nearly circular static PP-HMDSO deposit on a c-Si wafer substrate, displays optical interference rings; (b), one side of the corresponding film thickness profile shows a Gaussian-type thickness distribution. Here, $F_d = 0.15$ sccm was used, but the experiment was also repeated with lower HMDSO flow values, 0.01 and 0.08 sccm (see Table 1 below). On the basis of these three data sets only, it appears that PP-HMDSO deposition rate rises roughly proportionately with increasing F_d.

Data related to $F_d = 1$ sccm are not reported in Table 1 since the coatings were too powdery for reliable thickness determination with the profilometer.

3.2.2 | Chemical structure

Figure 8 shows four ATR-FTIR spectra corresponding to some of the present PP-HMDSO coatings resulting from $F_d = 0.01$, 0.08, 0.15, and 1 sccm monomer feed rate. Values of E_m for different F_d can be found in Table 2 below.

We will now proceed to comment on the IR spectra, with reference to Table 3, assignments of the main spectral features,[19,40–43] and to E_m values in Table 2.

Before doing so, we refer to an article entitled "Energetics of Reactions in a Dielectric Barrier Discharge with Argon Carrier Gas: V: Hydrocarbons"[44]; the authors, B. Nisol et al., reported a near-perfect linear relationship when plotting the peak value of E_m, $(E_m)_{max}$, versus the molecular weight of saturated hydrocarbon gases C_xH_{x+2} (x up to 8, n-octane). From this they concluded a plausible interpretation for $(E_m)_{max}$ to be the following, taking n-octane (C_8H_{18}) as an example: The respective (aliphatic) bond energies for C–C and C–H are 3.58 and 4.28 eV; assuming that every covalent bond in the molecule is broken, they found a total cumulative dissociation energy of 105.7 eV. However, the measured value, $(E_m)_{max} = 151.4$ eV, was nearly 50% higher; they postulated that this excess might be due to two causes, namely (i) electronic excitation of molecular fragments and (ii) recombination and redissociation reactions during the molecules' average residence time, τ, in the DBD plasma. In the large volume DBD reactor, where $\tau \sim 260$ ms, both these explanations

TABLE 1 PP-HMDSO coating thickness and deposition rates for various F_d values.

HMDSO flow rate [sccm], F_d	Thickness [μm]	Deposition rate [μm/min]
0.01	0.71	0.05
0.08	5.7	0.38
0.15	13.6	0.91

Abbreviation: HMDSO, hexamethyldisiloxane.

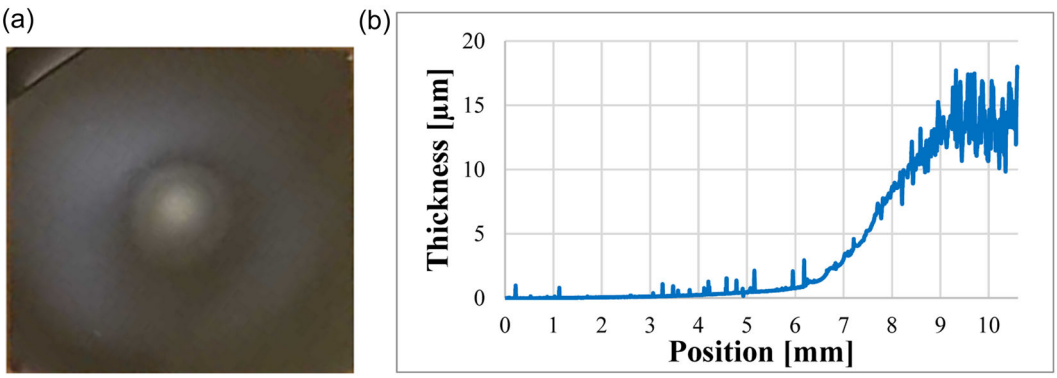

FIGURE 7 (a) Top view of a static PP-hexamethyldisiloxane (HMDSO) deposit on c-Si substrate, displaying optical interference rings; (b) corresponding Dektak thickness profile of $F_d = 0.15$ sccm coating.

seemed quite plausible because the very high collision rate at AP would certainly also enable ultra-rapid recombination/redissociation reactions to occur. A very rough calculation of τ for the case of the present CAPJet device based on dimensions drawn from Figure 2 yields an estimated value, $\tau \sim 1.7\ \mu s$; although many orders of magnitude lower, this does not exclude possible recombination/redissociation reactions from occurring here too.

At the highest value of E_m (smallest F_d in Table 2), total fragmentation of the HMDSO precursor molecules probably occurs, accompanied by near-total removal of methyl groups and other forms of bonded carbon, thus explaining the almost complete absence of relevant peaks in the FTIR spectrum.

At $E_m = 22.8$ eV per molecule, the spectrum exhibits several peaks associated with silicon bonds in the coating, such as Si–O–Si bending or stretching vibrations at 800 cm^{-1}, Si–OH stretching near 930 cm^{-1}, Si–O–Si asymmetric stretching at 1200–1000 cm^{-1}, and Si–OH stretching at 3100–3700 cm^{-1}. In the Si–O–Si asymmetric stretching band, the presence of two superimposed peaks can be clearly distinguished: in-phase asymmetric stretching AS1 near 1070 cm^{-1} and its out-of-phase counterpart at 1150 cm^{-1}. The weak peak at 1265 cm^{-1}, related to CH_3 stretching in Si–$(CH_3)_x$ ($x = 1,2,3$), is the only one to witness the presence of methyl groups, suggesting negligible carbon content in the coating deposited under this condition.

As E_m further decreases, new methyl-related peaks appear in the spectra: the CH_3 rocking or Si–$(CH_3)_2$ stretching band at 800 cm^{-1}, the CH_3 rocking or Si–$(CH_3)_3$ stretching band at 840 cm^{-1}. These, along with that at 1265 cm^{-1}, become progressively more pronounced as E_m diminishes still further. The AS2 "shoulder" in the band 1000–1200 cm^{-1} tends to become less pronounced, leading to an apparent "single peak" shape. The AS1 subpeak, in turn, shifts to a lower wavenumber (from 1070 to 1040 cm^{-1}). The described changes in the spectra have already been observed in the literature[19] and can be ascribed to a transition toward coatings with a more pronounced organic character. To summarize, highest E_m values gave rise to "silica-like" deposits, ones containing little or no residual carbon; on the contrary, low E_m values resulted in "organic-rich" coatings.[9]

It is noteworthy that Nisol[9] reported the same behavior as above in two spectra of their fig. 9(b), corresponding to PP-HMDSO films prepared in their large-area planar DBD reactor. The E_m values in their case were shown in brackets ("F":10.6 eV; "E": 112.6 eV). It could be clearly noticed that the lower E_m value was associated with pronounced methyl-related peaks (e.g., at 1265 cm^{-1}), while the higher one led to their greatly reduced presence.

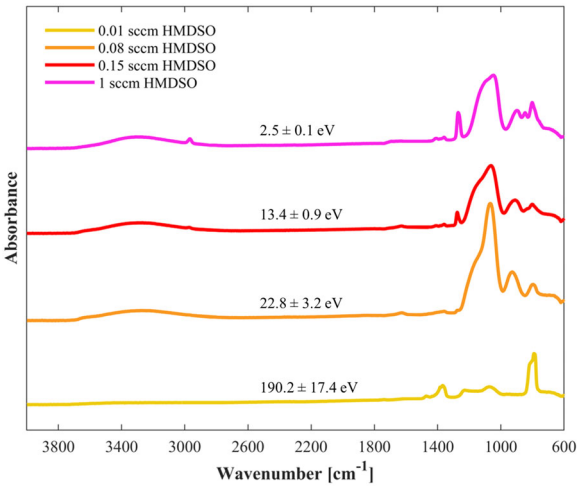

FIGURE 8 Attenuated total reflectance Fourier-transform infrared (ATR-FTIR) spectra of coatings deposited at 9 kV_{p-p} for different values of energy per precursor molecule, E_m.ATR-FTIR, attenuated total reflectance Fourier-transform infrared.

TABLE 3 Frequencies and assignments of the major absorption bands found in the IR spectra of coatings deposited from HMDSO.

Wavenumbers [cm^{-1}]	Accepted assignment
3700–3100	Si–OH stretching
2960	CH_3 stretching
1260–1250	CH_3 sym. deform. in Si-CH_3
	Si–$(CH_3)_x$ stretching ($x = 1,2,3$)
1070	Si–O–Si asymmetric stretching
1090–1020	Si–CH_2–Si wagging
870–930	Si–OH stretching
840	Si–C and CH_3 rocking
800	CH_3 rocking in $Si(CH_3)_{1,3}$
	Si–O–Si bending

Abbreviation: HMDSO, hexamethyldisiloxane.

TABLE 2 Values of energy per molecule, E_m, corresponding to shown F_d values.

Flow rate, F_d (sccm)	0.01	0.08	0.15	1
E_m (eV/molec)	190.2 ± 17.4	22.8 ± 3.2	13.4 ± 0.9	2.50 ± 0.1

The findings presented above strongly suggest the following very promising outcome: The "Delta-E method" that was developed, frequently tested, and proven for determining E_m in large area DBD plasma[9–11,44] has now apparently been successfully transferred to the current more challenging CAPJet geometry. This will be discussed further in the next (final) section.

4 | DISCUSSION AND CONCLUSIONS

A methodology, the so-called "Delta-E method," is presented for measuring the energy of reactions in a PP process initiated by a single-electrode cold atmospheric plasma jet (CAPJet) operating at 20.5 kHz and fed with Ar carrier gas and small amounts of HMDSO "monomer" additive. Values of energy per HMDSO precursor molecule, E_m (in eV/molec), are calculated by determining and solving equations relating to the "best" electrical equivalent circuit model. This current work has largely been motivated by that of Nisol et al., carried out for the case of a large area planar DBD reactor. To credibly demonstrate their physicochemical validity, these energy values, E_m, are correlated to appropriate measured properties of deposited PP-HMDSO thin films, assessed by ATR-FTIR spectroscopy and by profilometry.

Before discussing the results for PP-HMDSO presented in Section 3, it is useful to briefly re-examine the plasma science underlying the "Delta-E" and Lissajous figure methodologies used here, with particular reference to Sections 1.1 and 2.2 and articles cited therein. In Figure 4, we clearly noted the separations (ΔE_g) in energy dissipated per cycle, E_g, between "pure Ar" and "Ar + HMDSO" curves, similar to those first reported by Nisol for planar DBD geometries.[9–11,44] In those earlier articles, particularly in Nisol et al.[9], the authors had attributed the drop to the lower-E_g "Ar + monomer" curves to energy uptake by monomer molecules from the "reservoir" of energy stored in the flow of Ar* atoms, the lowest energy of metastable [Ar ($^3P_2$4s)] being 11.55 eV; the presumed dominant mechanism, of course, is Penning transfer during collisions. We believe that the term "reservoir" is justified: in spite of the short (ca. 100 ns) lifetime of Ar*, the duration of the current peaks in Ar DBD is quite long for $V_a = 9.0\ kV_{p\text{-}p}$, a large fraction (> 50%) of the AC half-period ($t \sim 24\ \mu s$ at 20.5 kHz).[9] Despite the quite short ($\tau \sim 1.7\ \mu s$) residence time of particles in the CAPJet plasma, we believe that Ar* are constantly replenished and that a quasi-steady-state concentration of Ar* exists, between 10^{11} and $10^{12}\ cm^{-3}$,[5] during the two current peaks of each voltage cycle. Based on section 7.1. "Excimer Lamps Based on Rare Gas Dimers" in Kogelschatz's review article,[2] "Computations indicate that under favorable conditions 40–80% of the discharge power can be converted to VUV radiation concentrated in the second excimer continua of Ar, Kr or Xe." This means not only that the creation of abundant Ar* species in AP DBD is highly efficient, but also that longer-lived (~ms) Ar_2* are among those Penning-active species. That high level of efficiency is again borne out in the more recent article by Kim et al.[12]

In the first of their articles in which absolute reaction energy values, ΔE_g, were being reported, Nisol et al.[10] stated that several other authors had published AP DBD studies designed to correlate PP deposition with W/FM, the Yasuda parameter defined in Section 1.2. Those energy values were usually based on the Lissajous figure method; for example, Kakaroglou et al.[16] entitled their article "Evaluation of the Yasuda parameter on atmospheric plasma deposition of allyl methacrylate": Using a DBD reactor of very similar design to that in,[9–11,44] also with Ar carrier gas, those authors did not distinguish between energy absorption with and without monomer, a characteristic common to all other published research known to us. Therefore, based on the "Delta-E method," one can state with confidence that W/FM was always overestimated and that such earlier correlations could be conducted only in a qualitative manner.

In the present work, the Lissajous figure measurements do not have that same shortcoming; instead, we believe that a quite different one is responsible for the much larger measured energy value, $E_g = 78$ eV versus 14 eV at 9 $kV_{p\text{-}p}$ in Figure 4, for the Lissajous and "Delta-E" methods, respectively, a ratio of 5.6. We tentatively explain this large difference as follows: Lissajous' method, obviously based on charge transfer, is incapable of distinguishing the dominant neutral Ar* Penning-based energy transfer processes discussed above, but it does measure the overall energy delivered to the discharge by the external power supply. In other words, the measured ratio (Lissajous/*delta-E* = 5.6) accounts for the fraction of electrical energy that goes toward producing Ar* and Ar_2* (VUV photons, in the case of UV lamp applications); presumably, the lower conversion efficiency here, ca. 18% versus earlier-cited 40%,[2] is the result of quenching by precursor and reaction product molecules in the mixture with pure Ar carrier gas.

In support of the interpretation offered above, as opposed to some other plasma-physical explanations, we present the following additional arguments: In Loffhagen et al.'s two modeling studies, sections dealing with energy loss due to HMDSO collisions as a function of the HMDSO fraction x (figs. 10A and 13 in Massines et al.[5] and Fateev et al.[6], respectively) show that electron- and ion collisions play negligibly small roles compared with Penning transfer from Ar* and Ar_2* for all x. In other words, neutral (Penning-) chemistry dominates the measured

energy loss mechanisms. This Penning dominance, rather than collisions with charged particles, electrons or ions, was also underlined by Fateev et al.[6]: the electron temperature, T_e, varied only slightly and electronic collisions gained importance only when NH_3 concentrations in Ar exceeded 3% (30,000 ppm). At the very low precursor (or "monomer") concentrations used here and in Nisol's articles, typically a few tens to some hundreds of ppm, the plasma properties (T_e and n_e) are little affected; that is, the dissociation and ionization by Penning reaction involving a transfer between the excited Ar states and the precursor molecules greatly dominate.

Returning to the discussion of PP-HMDSO results in Section 3 above, the magnitudes and trends of the presented E_m values appear to be in realistic agreement with the coatings' properties, which lends support to the validity of the "Delta-E method" for use with the AP single electrode CAPjet. Nonetheless, to further test its reliability, we now add some considerations about how measured E_m values relate to known energies required to break covalent bonds in the HMDSO molecule. For simplicity, we neglect possible modifications of bond energies in the reactive plasma environment, as well as possible photochemical contributions due to the energetic VUV photons in AP Ar discharges.[2,37]

The main bond energies in HMDSO are 3.5 eV for C–H, 4.53 eV for Si–C, and 8.31 eV for Si–O.[40,41] This means that E_m values of 22.8, 13.4, and 2.5 (all in eV/molec, obtained for precursor flow rates $F_d = 0.08$, 0.15, and 1 sccm, respectively) are of comparable magnitudes and can serve to interpret fragmentation mechanisms, even though detailed pathways are beyond the scope of this work.

Clearly, $E_m = 22.8$ eV/molec suffices to break all the abovementioned bond types; this can help explain the presence of FTIR features mostly related to "inorganic" coatings. As the energy decreases to 13.4 eV/molec, the bond dissociation is less intense, and more methyl groups can be conserved in the final coating. Coatings deposited for an E_m of 2.5 eV exhibit the most organic character, suggesting an extremely low fragmentation of the precursor in the coating. This is coherent with the bond energies in the HMDSO molecules, since 2.5 eV is around the minimum values which are needed to abstract hydrogen or methyl groups. Among the values of E_m investigated in this work, 190.2 eV/molec corresponds to the condition where the maximum transfer of energy from the plasma discharge to the precursor molecules occurs. Since the sum of all the bond energies in the HMDSO molecule is around 105 eV, the ATR-FTIR spectrum observed at 190.2 eV/molec can be reasonably explained as resulting from the total breakage of all the constituent bonds.

As earlier demonstrated by Nisol et al. for planar DBD, it is therefore shown here too that realistic E_m values can be successfully obtained also for the CAPJet case, a priori more challenging in many ways than for the planar geometry. For example, a monotonic decrease of E_m as a function of increasing precursor flow rate, F_d, is observed for two applied voltages, 5.5 and 9 kV_{p-p}, numerical values being in good agreement with Nisol's.[9] It is remarkable that the peak values of E_m in both cases have comparable numerical values, ~190 and 131 eV, respectively. Furthermore, ATR-FTIR spectra of coatings deposited under different F_d conditions exhibit very comparable features in both the planar DBD and CAPJet cases, not inconsistent with corresponding E_m values: as E_m increases, so also does fragmentation of the HMDSO precursor in the discharge plasma, and the conservation of functional groups (methyl groups and other forms of bonded carbon) in the PP-HMDSO coating is reduced. The deposition rate of films, determined by profilometry, also follows expectations by increasing with rising F_d, despite greatly and systematically differing chemical compositions. All of these described qualitative and semiquantitative observations, taken together, support the validity of the currently developed "Delta-E method."

The energy results obtained with the "Delta-E method" were also compared with those from the Lissajous figures method. While the current "Delta-E method" leads to realistic E_m values, judged in terms of known chemical bond energies and measured properties of the coatings, energies derived from the Lissajous method are several times too large (typically 6× in the present example) to be physically meaningful. This has been explained here by the fact that only the fraction of delivered total energy going toward creating metastable Ar* and Ar_2* species needs to be considered here: that fraction is responsible for those metastable Ar* species that give rise to the dominant Penning (ionization and dissociation) reactions. In other words, this comparison with the Lissajous figures method, a technique that is still frequently encountered in the literature, often with little questioning, presents an encouraging confirmation of the current "Delta-E" method's potentialities for use with CAPJet, but also more generally with AP DBD plasma-chemical processes.

ACKNOWLEDGMENTS

The authors (Stephan Reuter and Michael R. Wertheimer) gratefully acknowledge funding support from the Natural Sciences and Engineering Research Council (NSERC) of Canada. Stephan Reuter also acknowledges financial support from the Fond de recherche du Québec and the TransMedTech Institute through its main financial partner, the Apogee Canada First Research Excellence Fund. Furthermore, Giulia

Laghi acknowledges support from the European COST Action CA20114 "Therapeutical applications of cold plasmas" (PlasTHER).

DATA AVAILABILITY STATEMENT

The data that support the findings of this study are available from the corresponding author upon reasonable request.

ORCID

Giulia Laghi http://orcid.org/0000-0003-1815-4342
Stephan Reuter http://orcid.org/0000-0002-4858-1081
Matteo Gherardi http://orcid.org/0000-0001-6995-6754
Michael R. Wertheimer http://orcid.org/0000-0002-7718-1757

REFERENCES

[1] R. Bartnikas, *J. Phys. D: Appl. Phys.* **1968**, *1*, 659–661.
[2] U. Kogelschatz, *Plasma Chem. Plasma Process.* **2003**, *23*, 1–46.
[3] R. Brandenburg, K. H. Becker, K.-D. Weltmann, *Plasma Chem. Plasma Process.* **2023**. https://doi.org/10.1007/s11090-023-10364-5
[4] S. Okazaki, M. Kogoma, M. Uehara, Y. Kimura, *J. Phys. D: Appl. Phys.* **1993**, *26*, 889–892.
[5] F. Massines, N. Gherardi, N. Naudé, P. Ségur, *Plasma Phys. Controlled Fusion* **2005**, *47*, B577–B588.
[6] A. Fateev, F. Leipold, Y. Kusano, B. Stenum, E. Tsakadze, H. Bindslev, *Plasma Processes Polym.* **2005**, *2*, 193–200.
[7] D. Loffhagen, M. M. Becker, A. K. Czerny, J. Philipp, C.-P. Klages, *Contrib. Plasma Phys.* **2018**, *58*, 337–352.
[8] D. Loffhagen, M. M. Becker, D. Hegemann, B. Nisol, S. Watson, M. R. Wertheimer, C.-P. Klages, *Plasma Processes Polym.* **2020**, *17*(1), 190016911.
[9] B. Nisol, S. Watson, S. Lerouge, M. R. Wertheimer, *Plasma Processes Polym.* **2016**, *13*, 557–564.
[10] B. Nisol, H. Gagnon, S. Lerouge, M. R. Wertheimer, *Plasma Processes Polym.* **2016**, *13*, 366–374.
[11] S. Watson, B. Nisol, S. Lerouge, M. R. Wertheimer, *Langmuir* **2015**, *31*, 10125–10129.
[12] J. Kim, A. E. Mironov, J. H. Cho, D. S. Sievers, C. M. Herring, S. Park, P. P. Sun, Z. Liang, W. Chen, S. J. Park, J. G. Eden, *Plasma Processes Polym.* **2022**, *19*, e2200075.
[13] M. R. Ch. Oehr, Wertheimer, *Polym. 19* **2022**, *2277025*, 2.
[14] H. Yasuda, T. Hirotsu, *J. Polym. Sci. Polym. Chem. Ed.* **1978**, *16*, 743–759.
[15] H. K. Yasuda, *Plasma Processes Polym.* **2005**, *2*, 293–304.
[16] A. Kakaroglou, B. Nisol, K. Baert, I. De Graeve, F. Reniers, G. Van Assche, H. Terryn, *RSC Adv.* **2015**, *5*, 27449–27457.
[17] D. Hegemann, B. Nisol, S. Watson, M. R. Wertheimer, *Plasma Chem. Plasma Process.* **2017**, *37*, 257–271.
[18] D. Hegemann, E. Körner, S. Chen, J. Benedikt, A. von Keudell, *Appl. Phys. Lett.* **2012**, *100*, 051601.
[19] R. Morent, N. De Geyter, S. Van Vlierberghe, P. Dubruel, C. Leys, E. Schacht, *Surf. Coat. Technol.* **2009**, *203*, 1366–1372.
[20] D. Merche, N. Vandencasteele, F. Reniers, *Thin Solid Films* **2012**, *520*, 4219–4236.
[21] F. Massines, C. Sarra-Bournet, F. Fanelli, N. Naudé, N. Gherardi, *Plasma Processes Polym.* **2012**, *9*, 1041–1073.
[22] Q. Chen, Y. Zhang, E. Han, Y. Ge, *J. Vac. Sci. Technol., A* **2006**, *24*, 2082–2086.
[23] J. Pulpytel, V. Kumar, P. Peng, V. Micheli, N. Laidani, F. Arefi-Khonsari, *Plasma Processes Polym.* **2011**, *8*, 664–675.
[24] H. Kakiuchi, K. Higashida, T. Shibata, H. Ohmi, T. Yamada, K. Yasutake, *J. Non-Cryst. Solids* **2012**, *358*, 2462–2465.
[25] J. Li, Q. Yuan, X. Chang, Y. Wang, G. Yin, C. Dong, *Plasma Sci. Technol. 19* **2017**, *045505*, 7.
[26] Y. C. Lin, M. J. Wang, *Jpn. J. Appl. Phys.* **2019**, *58*, SAAC01.
[27] Z. Fang, T. Shao, J. Yang, C. Zhang, *Eur. Phys. J. D* **2016**, *70*, 8.
[28] T. C. Manley, *Trans. Electrochem. Soc.* **1943**, *84*, 83.
[29] F. Peeters, T. Butterworth *Atmospheric Pressure Plasma - From Diagnostics to Applications* (Eds. A. Nikiforov, Z. Chen), IntechOpen Limited, London, UK **2018**, pp. 27.
[30] F. Barletta, C. Leys, V. Colombo, M. Gherardi, N. Britun, R. Snyders, A. Nikiforov, *Plasma Processes Polym.* **2020**, *17*, 6.
[31] T. Gallingani, E. Resca, M. Dominici, G. Gavioli, R. Laurita, A. Liguori, G. Mari, L. Ortolani, E. Pericolini, A. Sala, G. Laghi, T. Petrachi, G. F. Arnauld, L. Accorsi, R. Rizzoli, V. Colombo, M. Gherardi, E. Veronesi, *PLoS One* **2023**, *18*, e0282059.
[32] M. Archambault-Caron, H. Gagnon, B. Nisol, K. Piyakis, M. R. Wertheimer, *Plasma Sources Sci. Technol.* **2015**, *24*, p 04500416.
[33] S. Watson, B. Nisol, H. Gagnon, M. Archambault-Caron, F. Sirois, M. R. Wertheimer, *IEEE Trans. Plasma Sci.* **2019**, *47*, 2680–2688.
[34] A. V. Pipa, J. Koskulics, R. Brandenburg, T. Hoder, *Rev. Sci. Instrum. 83* **2012**, *115112*, 7.
[35] A. Pipa, R. Brandenburg, *Atoms* **2019**, *7*, 14.
[36] R. Brandenburg, M. Schiorlin, M. Schmidt, H. Höft, A. V. Pipa, V. Brüser, *Plasma* **2023**, *6*, 162–180.
[37] R. Magnan, G. Hagelaar, M. Chaker, F. Massines, *Plasma Sources Sci. Technol.* **2021**, *30*, 015010.
[38] M. Dünnbier, M. M. Becker, S. Iseni, R. Bansemer, D. Loffhagen, S. Reuter, K.-D. Weltmann, *Plasma Sources Sci. Technol.* **2015**, *24*, 065018.
[39] M. A. Lieberman, A. J. Lichtenberg, *Principles of Plasma Discharges and Materials Processing*, Wiley, New York **1994**.
[40] A. M. Wrobel, M. R. Wertheimer *Plasma-Polymerized Organosilicones and Organometallics", in "Plasma Deposition, Treatment and Etching of Polymers Films* (Ed. R., d'Agostino), Academic Press, New York **1990**, pp. 163–268.
[41] M. T. Kim, *Thin Solid Films* **1997**, *311*, 157–163.
[42] G. Socrates, *Infrared and Raman Characteristic Group Frequencies - Tables and Charts*, John Wiley & Sons Ltd, West Sussex — UK **2001**.
[43] A. Grill, D. A. Neumayer, *J. Appl. Phys.* **2003**, *94*, 6697–6707.
[44] B. Nisol, S. Watson, S. Lerouge, M. R. Wertheimer, *Plasma. Process. Polym.* **2017**, *14*(1600191), 9p.

How to cite this article: G. Laghi, S. Watson, S. Reuter, M. Gherardi, M. R. Wertheimer, *Plasma. Process. Polym.* **2023**, e2300134. https://doi.org/10.1002/ppap.202300134